

CHAPTER 5

Characteristics of the Circular Patch Antenna

5.1 Geometry and Coordinate Systems

The circular patch antenna is extensively used in practice. The geometry is shown in Fig. 5.1. It is characterized by the radius (a), the substrate thickness (t) and its relative permittivity (ϵ_r). Spherical coordinate system is used to describe a field point $P(r, \theta, \phi)$ while cylindrical coordinate system is used to describe a source point $P'(\rho, \varphi, z)$.

5.2 Characteristics of Normal Modes

5.2.1 Internal Fields

The normal modes refer to the source free fields which can exist in the region between the patch and the ground plane. This region is modeled as a cavity bounded by electric walls on the top and bottom and magnetic walls on the sides. As discussed in sections 3.3 and 3.4, under the assumption that the thickness is much less than the wavelength, the electric field has only a vertical component E_z which is independent of z and satisfies the homogeneous equation

$$(\nabla^2 + k_d^2)E_z = 0 \quad (3.10)$$

and the boundary condition $\vec{H}_t = 0$ on the side walls of the cavity. In cylindrical coordinates, Eq. (3.10) reads

$$\frac{1}{\rho} \frac{\partial}{\partial \rho} \left(\rho \frac{\partial E_z}{\partial \rho} \right) + \frac{1}{\rho^2} \frac{\partial^2 E_z}{\partial \varphi^2} + \frac{\partial^2 E_z}{\partial z^2} = -k_d^2 E_z \quad (5.1)$$

Due to the assumption of the cavity model, $\frac{\partial^2 E_z}{\partial z^2} = 0$.

Using the method of the separation of variables, we let

$$E_z = P(\rho)Q(\varphi) \quad (5.2)$$

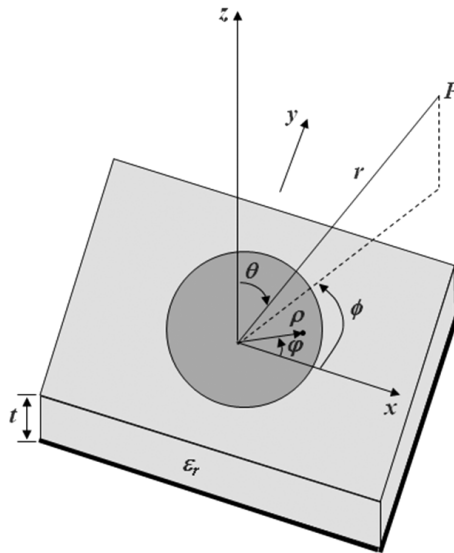


Fig. 5.1 Geometry of a circular patch antenna.

Equation (5.1) becomes

$$\frac{\rho}{P} \frac{\partial}{\partial \rho} \left(\rho \frac{\partial P}{\partial \rho} \right) + k_d^2 \rho^2 = -\frac{1}{Q} \frac{\partial^2 Q}{\partial \varphi^2} \quad (5.3)$$

Since the right hand side depends on φ only and the left hand side depends on ρ only, we have the following equations for the functions Q and P :

$$\frac{1}{Q} \frac{\partial^2 Q}{\partial \varphi^2} = -n^2 \quad (5.4)$$

and

$$\rho^2 \frac{\partial^2 P}{\partial \rho^2} + \rho \frac{\partial P}{\partial \rho} + [(k_d \rho)^2 - n^2] P = 0 \quad (5.5)$$

The solution for Q is

$$Q = c_1 \cos n\varphi \quad (5.6)$$

where n is an integer since Q must be periodic with period 2π .

The solution for P is

$$P = c_2 J_n(k_d \rho) + c_3 Y_n(k_d \rho) \quad (5.7)$$

where J_n is the Bessel function of the first kind of order n and Y_n is the Bessel function of the second kind of order n .

Since fields are finite at $\rho = 0$, $c_3 = 0$.

Thus

$$E_z = E_0 J_n(k_d \rho) \cos n\varphi \tag{5.8}$$

From Maxwell's equations, we obtain

$$H_\rho = -j \frac{\omega \varepsilon n}{k^2 \rho} E_0 J_n(k_d \rho) \sin n\varphi \tag{5.9}$$

$$H_\varphi = -j \frac{\omega \varepsilon}{k} E_0 J'_n(k_d \rho) \cos n\varphi \tag{5.10}$$

where $J'_n(k_d \rho)$ is the derivative of $J_n(k_d \rho)$ with respect to the argument $k_d \rho$.

Applying the magnetic wall boundary condition, we have

$$H_\varphi = 0|_{\rho=a} \Rightarrow J'_n(k_d a) = 0 \tag{5.11}$$

Let the roots of (5.11) be X_{nm} . Then the eigenvalues of k_d , denoted by k_{nm} , are:

$$k_{nm} = \frac{X_{nm}}{a} \tag{5.12}$$

5.2.2 Resonant Frequencies

The resonant frequency of a TM_{nm} mode is

$$f_{nm} = \frac{X_{nm}}{2\pi a \sqrt{\mu_0 \varepsilon}} = \frac{X_{nm} c}{2\pi a \sqrt{\varepsilon_r}} \tag{5.13}$$

The first five values of X_{nm} are:

(n, m)	(1,1)	(2,1)	(0,2)	(3,1)	(1,2)
X_{nm}	1.841	3.054	3.832	4.201	5.331

Equation (5.13), which is based on the perfect magnetic wall assumption, yields resonant frequencies which differ from measurements by about 20%. To take into account the effect of fringing field, an effective radius was introduced. This was obtained by considering the radius of an ideal circular parallel plate capacitor which would yield the same static capacitance after fringing is taken into account. A detailed calculation yields the

formula [1, 2]

$$a_e = a \left[1 + \frac{2t}{\pi a \epsilon_r} \ln \left(\frac{\pi a}{2t} + 1.7726 \right) \right]^{1/2} \quad (5.14)$$

Using a_e , the resonant frequency formula becomes

$$f_{nm} = \frac{X_{nm}c}{2\pi a_e \sqrt{\epsilon_r}} \quad (5.15)$$

Equation (5.15) yields theoretical resonant frequencies which are within 2.5% of measured values.

5.2.3 Radiation Fields

The surface magnetic current density on the side walls of the cavity is given by

$$\vec{M} = 2\vec{E}|_{\rho=a} \times \hat{n} = 2E_z|_{\rho=a} \hat{\phi} \quad (5.16)$$

Since \vec{M} is expressed in cylindrical coordinates, it has to be transformed to spherical coordinates before deriving the far fields (radiation fields):

$$\begin{bmatrix} M_r \\ M_\theta \\ M_\phi \end{bmatrix} = \begin{bmatrix} \sin \theta \cos(\varphi - \phi) & -\sin \theta \sin(\varphi - \phi) & \cos \theta \\ \cos \theta \cos(\varphi - \phi) & -\cos \theta \sin(\varphi - \phi) & \sin \theta \\ \sin(\varphi - \phi) & \cos(\varphi - \phi) & 0 \end{bmatrix} \begin{bmatrix} M_\rho \\ M_\varphi \\ M_z \end{bmatrix} \quad (5.17)$$

In our problem, $M_\rho = M_z = 0$.

The electric vector potential is

$$\vec{F}(\vec{r}) = \frac{\epsilon_0}{4\pi} \iint (M_r \hat{r} + M_\theta \hat{\theta} + M_\phi \hat{\phi}) \frac{e^{-jk_0|\vec{r}-\vec{r}'|}}{|\vec{r}-\vec{r}'|} d\sigma' \quad (5.18)$$

where integration is over the area of the fictitious magnetic side wall.

The far fields are given by

$$E_\theta = -j\omega\eta_0 F_\phi \quad (5.19a)$$

$$E_\phi = j\omega\eta_0 F_\theta \quad (5.19b)$$

where

$$F_\theta = \frac{\epsilon_0}{4\pi} \iint [-\cos \theta \sin(\varphi - \phi) M_\varphi] \frac{e^{-jk_0|\vec{r}-\vec{r}'|}}{|\vec{r}-\vec{r}'|} d\sigma' \quad (5.20)$$

$$F_\phi = \frac{\epsilon_0}{4\pi} \iint [\cos(\varphi - \phi) M_\varphi] \frac{e^{-jk_0|\vec{r}-\vec{r}'|}}{|\vec{r}-\vec{r}'|} d\sigma' \quad (5.21)$$

After lengthy manipulation, we arrived at the result:

$$E_{\theta} = j^n \frac{tE_0 J_n(k_{nm}a) a k_0}{2} \frac{e^{-jk_0 r}}{r} \times \cos n\phi [J_{n+1}(ak_0 \sin \theta) - J_{n-1}(ak_0 \sin \theta)] \quad (5.22)$$

$$E_{\phi} = j^n \frac{tE_0 J_n(k_{nm}a) a k_0}{2} \frac{e^{-jk_0 r}}{r} \times \cos \theta \sin n\phi [J_{n+1}(ak_0 \sin \theta) + J_{n-1}(ak_0 \sin \theta)] \quad (5.23)$$

5.3 Coaxial Fed Circular Patch

5.3.1 Internal and Radiation Fields

Figure 5.2 shows a coaxial feed at a distance d from the center of the patch of radius a . The feed is modeled by a z -directed current ribbon of some effective angular width $2w$. Hence

$$\vec{J} = \hat{z} J(\varphi) \delta(\rho - d) / d \quad (5.24)$$

where

$$J(\varphi) = \begin{cases} J & \pi - w < \varphi < \pi + w \\ 0 & \text{elsewhere} \end{cases} \quad (5.25)$$

The effective arc width $2wd$ is a parameter chosen such that good agreement between the theoretical and experimental impedances are obtained. Usually, it is several times the diameter of the inner conductor.

Using the formulas developed in Chapter 3, the fields under the circular cavity are found to be given by:

$$E_z = j\omega\mu_0 J \sum_m \sum_n A_{nm} J_n(k_{nm}\rho) \cos n(\varphi - \pi) \quad (5.26)$$

where

$$A_{nm} = \frac{2\varepsilon_n \sin nw J_n(k_{nm}d) \cos(n\pi)}{n\pi J_n^2(k_{nm}a) (k_d^2 - k_{nm}^2) (a^2 - n^2/k_{nm}^2)} \quad (5.27)$$

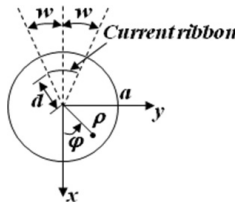


Fig. 5.2 Top view of a coaxial fed circular patch.

$$\varepsilon_n = \begin{cases} 1 & n = 0 \\ 2 & n \neq 0 \end{cases} \quad (5.28)$$

$$H_\varphi = Jk_d^2 \sum_m \sum_n \frac{A_{nm}}{k_{nm}} J'_n(k_{nm}\rho) \cos n(\varphi - \pi) \quad (5.29)$$

$$H_\rho = \frac{Jk_d^2}{\rho} \sum_m \sum_n \frac{nA_{nm}}{k_{nm}^2} J_n(k_{nm}\rho) \sin n(\varphi - \pi) \quad (5.30)$$

The fields in the far zone (radiation fields) are evaluated to be

$$E_\theta = j\omega\mu_0 \frac{Jtak_0}{2} \frac{e^{-jk_0r}}{r} \sum_m \sum_n j^n A_{nm} J_n(k_{nm}a) \cos n\phi \times [J_{n+1}(ak_0 \sin \theta) - J_{n-1}(ak_0 \sin \theta)] \quad (5.31)$$

$$E_\phi = j\omega\mu_0 \frac{Jtak_0}{2} \frac{e^{-jk_0r}}{r} \times \cos \theta \sum_m \sum_n j^n A_{nm} J_n(k_{nm}a) \sin n\phi \times [J_{n+1}(ak_0 \sin \theta) + J_{n-1}(ak_0 \sin \theta)] \quad (5.32)$$

5.3.2 Losses and Q

Based on the resonance approximation, the dielectric, copper, and radiation losses and the total energy stored when the excitation frequency is near the resonant frequency of mode (n, m) are given by

$$P_d = (\omega\mu_0 J)^2 \frac{t\delta A_{nm}^2}{8\mu_0 f} J_n^2(k_{nm}a) [(k_{nm}a)^2 - n^2] \quad (5.33)$$

$$P_c = J^2 \left(\frac{\pi f \mu_0}{\sigma} \right)^{1/2} A_{nm}^2 \frac{\pi}{2} J_n^2(k_{nm}a) [(k_{nm}a)^2 - n^2] \quad (5.34)$$

$$P_r = (\omega\mu_0 J)^2 \frac{(tak_0)^2 A_{nm}^2 J_n^2(k_{nm}a)}{1920} I_1 \quad (5.35)$$

$$W_T = 2W_e = \frac{\varepsilon}{2} \iiint |E_z|^2 d\tau' = \frac{P_d}{\omega\delta} \quad (5.36)$$

where σ is the conductivity of the patch and the ground plane, and

$$I_1 = \int_0^\pi \left\{ [J_{n+1}(ak_0 \sin \theta) - J_{n-1}(ak_0 \sin \theta)]^2 + \cos^2 \theta [J_{n+1}(ak_0 \sin \theta) + J_{n-1}(ak_0 \sin \theta)]^2 \right\} \sin \theta d\theta \quad (5.37)$$

The total Q factor

$$Q_T = \frac{\omega W_T}{P_d + P_c + P_r} \tag{5.38}$$

The effective loss tangent and the effective wavenumber in the substrate are given by

$$\delta_{eff} = \frac{1}{Q_T} = \delta + \frac{1}{t\sqrt{\sigma\pi\mu_0 f}} + \frac{ta^2k_0^2f\mu_0I_1}{240[(k_{nm}a)^2 - n^2]} \tag{5.39}$$

$$k_{eff} = k_0\sqrt{\varepsilon_r(1 - j\delta_{eff})} \tag{5.40}$$

5.3.3 Input Impedance

The input impedance

$$Z = R + jX = \frac{V_{in}}{I} \tag{5.41}$$

where

$$V_{in} = -\int_0^t E_{av}dz = -E_{av}t \tag{5.42}$$

$$E_{av} = \frac{1}{2w} \int_{\pi-w}^{\pi+w} E_z|_{\rho=d}d\varphi \tag{5.43}$$

$$I = \int_0^{2\pi} \int_0^a J(\varphi)\rho d\rho d\varphi = 2wJ \tag{5.44}$$

After evaluating the integrals, we obtain

$$Z = -j\omega\mu_0t \left[\sum_{m=1}^{\infty} \frac{1}{\pi a^2} \frac{J_0^2(k_{0m}d)}{J_0^2(k_{0m}a)} + \sum_{m=1}^{\infty} \sum_{n=1}^{\infty} \frac{2}{\pi} \frac{(\sin nw)^2}{(nw)^2} \frac{J_n^2(k_{nm}d)/J_n^2(k_{nm}a)}{(a^2 - \frac{n^2}{k_{nm}^2})(k_{eff}^2 - k_{nm}^2)} \right] \tag{5.45}$$

In the above equation for Z , the effective wavenumber k_{eff} has replaced k_d and the effective loss tangent has been utilized.

5.4 Illustrative Results

5.4.1 Magnetic Current Distribution

The magnetic current distribution around the edge of the circular disc for the n -th mode is proportional to $\cos n(\varphi - \pi)$. This is illustrated in Fig. 5.3 for $n = 0, 1, 2$ and 3 [2].

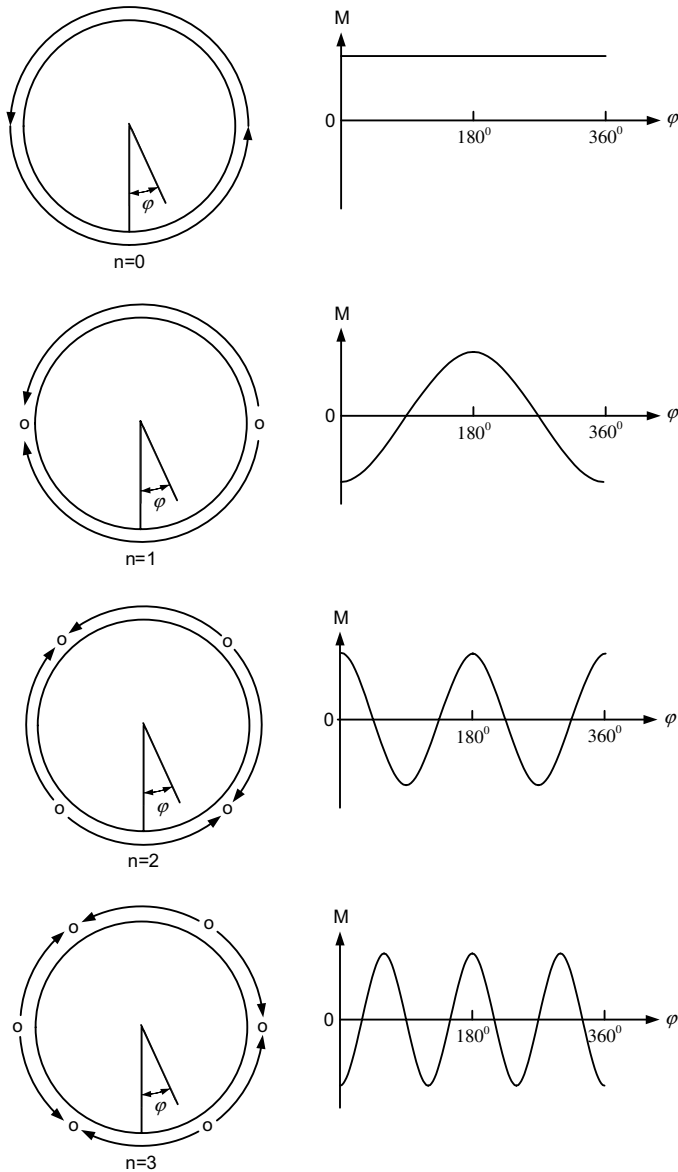


Fig. 5.3 The magnetic current distribution of circular disc for $n = 0, 1, 2$ and 3 . (Reproduced by permission from I. J. Bahl and P. Bhartia "Microstrip Antenna", Norwood, M.A. Artech House, Inc. 1980)

5.4.2 Radiation patterns

The radiation patterns of the lowest two modes, TM_{11} and TM_{21} , are shown in Fig. 5.4 from the paper by Lo *et al.* [3]. The TM_{11} mode radiates strongest in the broadside direction while the TM_{21} mode has a null in the broadside direction. The radiation patterns of the higher order modes (0, 2) and (3, 0) also exhibit nulls in the broadside direction (not shown).

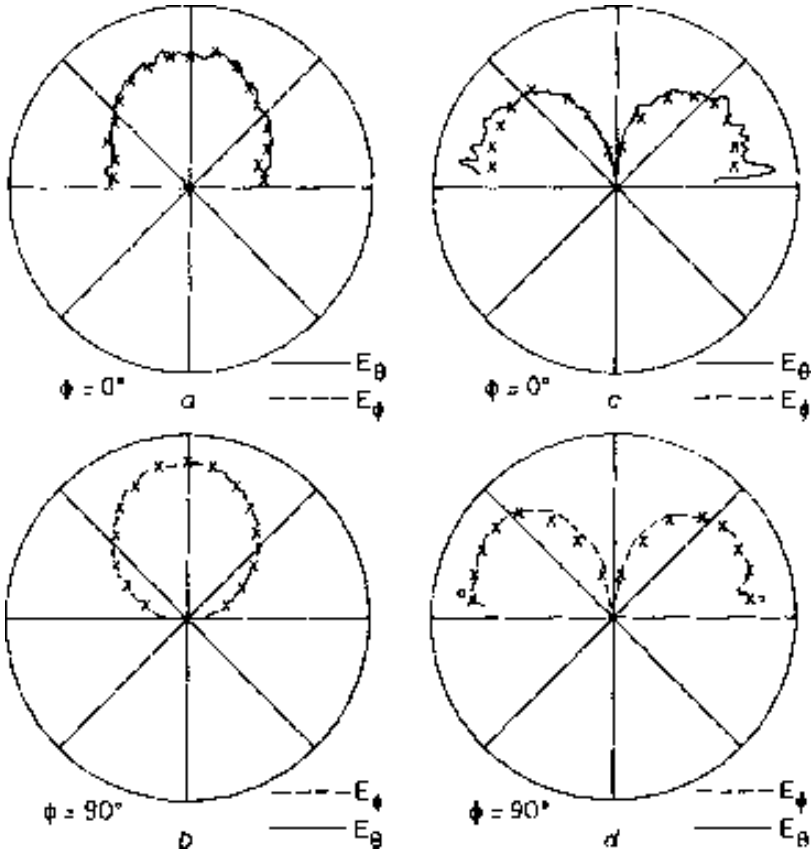


Fig. 5.4 Theoretical (x) and measured radiation patterns in the $\phi = 0^\circ$ and $\phi = 90^\circ$ planes of a circular patch with radius $a = 6.75$ cm, $\epsilon_r = 2.32$. (a) and (b) at 794 MHz of mode (1,1), (c) and (d) at 1324 MHz if mode (2,1) (From [3]. © 1981 IEEE Reprinted with permission.)

5.4.3 Radiation Efficiency, Directivity, Gain, Total Q and Bandwidth

Based on the equations obtained in this chapter, the radiation efficiency, directivity, gain, total Q and bandwidth are illustrated in Figs. 5.5–5.9 for the broadside mode TM_{11} [4]. The characteristics are qualitatively similar to the lowest two modes of the rectangular patch.

5.4.4 Input Impedance

Richards *et al.* [5] reported calculated and measured values of the input impedance as a function of radial feed position. This is shown in Fig. 5.10 for the TM_{11} mode. It is seen that the input resistance is largest when fed at the edge of the patch, but it can attain the convenient value of 50Ω when the feed location is chosen properly.

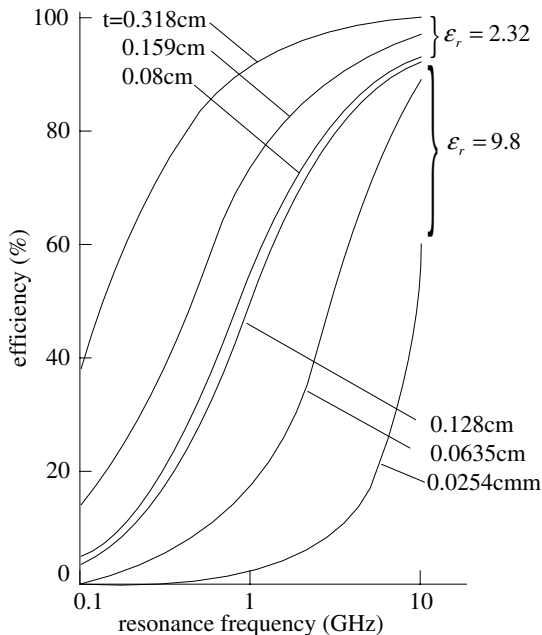


Fig. 5.5 Radiation efficiency versus frequency for the TM_{11} mode of the circular patch with $\sigma = 5.8 \times 10^7 \text{ S/m}$, $\delta = 0.0005$ and (i) $\epsilon_r = 2.32$, $t = 0.318$, 0.159 , 0.0795 cm; (ii) $\epsilon_r = 9.8$, $t = 0.127$, 0.0635 , 0.0254 cm. (From [4], © 1989, IET, reprinted with permission)

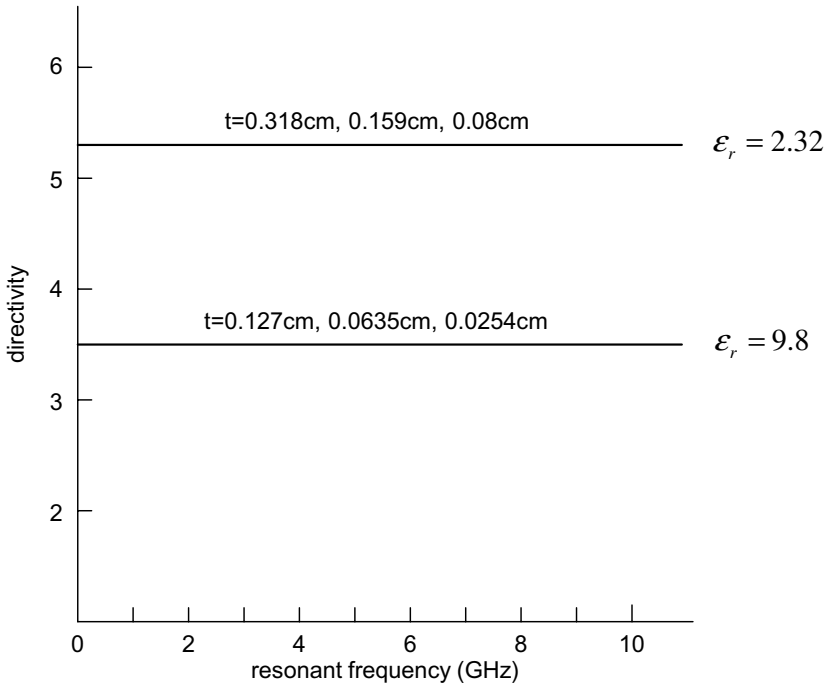


Fig. 5.6 Directivity versus resonant frequency for the TM_{11} mode of the circular patch: (i) $\epsilon_r = 2.32$, $t = 0.318, 0.159, 0.0795$ cm; (ii) $\epsilon_r = 9.8$, $t = 0.127, 0.0635, 0.0254$ cm. (From [4], © 1989, IET, reprinted with permission)

Dahele and Lee [6] have studied experimentally the effect of substrate thickness on input impedance. Their results are shown in Fig. 5.11.

5.5 Cross Polarization Characteristics

The cross polarization level is an important consideration when two orthogonal polarizations are used to provide two communication channels for each frequency band, in order to utilize the frequency spectrum efficiently. For the circular patch, this was studied by Lee *et al.* [7]. The coordinate system used in their study is shown in Fig. 5.12.

In a specified plane, the cross polarization level is defined as the ratio of the maximum magnitude of E_{copol} to the maximum magnitude of E_{xpol} . The third definition of Ludwig is used to define the copolarization E_{copol}

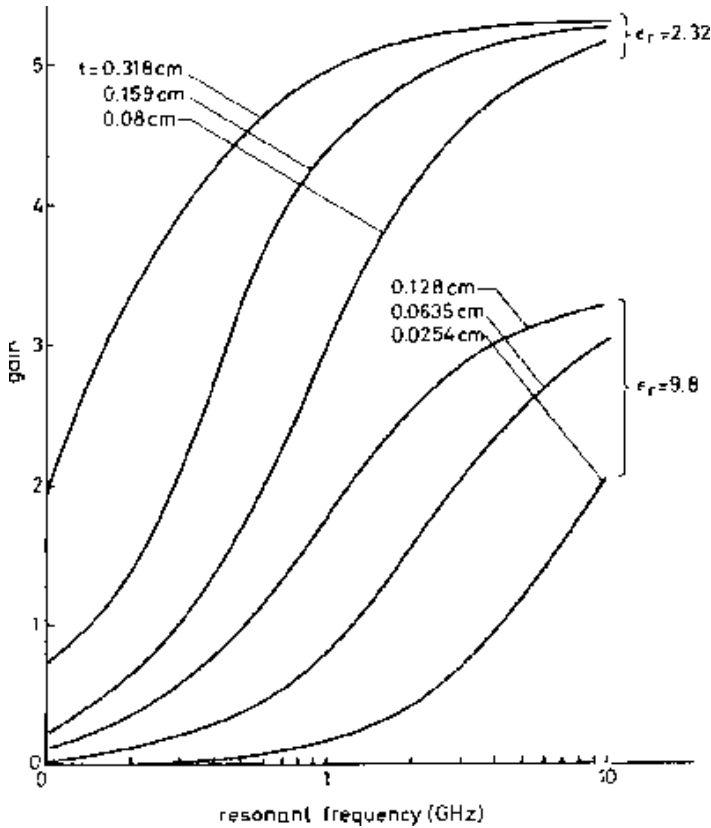


Fig. 5.7 Gain versus resonant frequency for the TM_{11} mode of the circular patch with $\sigma = 5.8 \times 10^7$ S/m, $\delta = 0.0005$ (i) $\epsilon_r = 2.32$, $t = 0.318, 0.159, 0.0795$ cm; (ii) $\epsilon_r = 9.8$, $t = 0.127, 0.0635, 0.0254$ cm. (From [4], © 1989, IET, reprinted with permission)

and the crosspolarization E_{xpol} [8]:

$$E_{copol} = E_\theta \cos \phi - E_\phi \sin \phi \quad (5.46a)$$

$$E_{xpol} = E_\theta \sin \phi + E_\phi \cos \phi \quad (5.46b)$$

It follows from Eq. (5.46) that, in the E plane ($\phi = 0^\circ$), $E_\phi = 0$ and there is no cross polarized fields due to orthogonal modes.

Radiation patterns in the H plane ($\phi = 90^\circ$) for both copolar and crosspolar components are given in Fig. 5.13 for two feed positions, when the antenna is excited at the resonance frequency of the TM_{11} mode. It is noted that the copolar components are maximum in the broadside direction

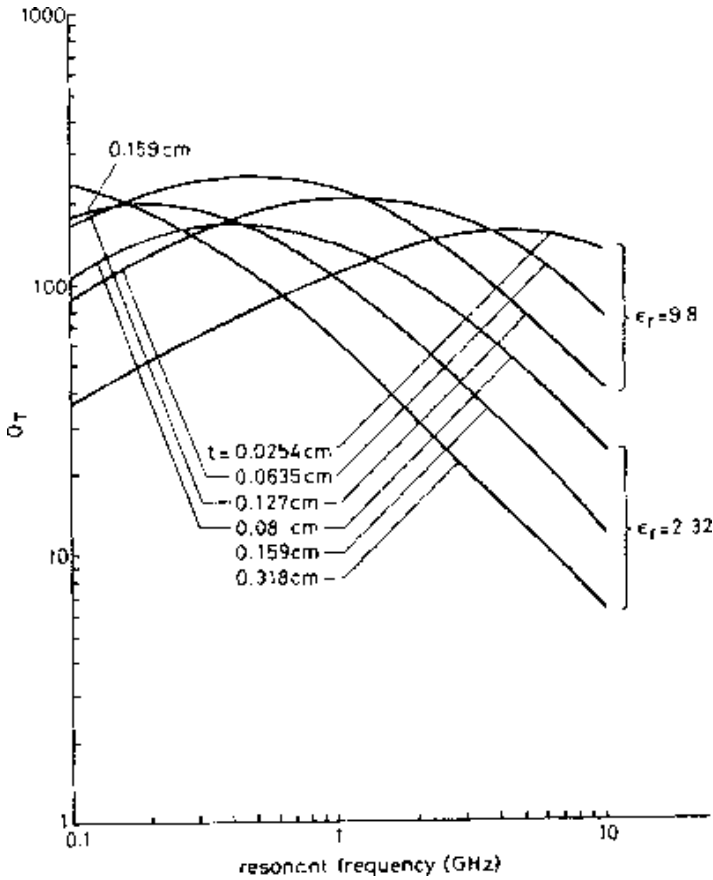


Fig. 5.8 Total Q versus resonant frequency for the TM_{11} mode of the circular patch with $\sigma = 5.8 \times 10^7$ S/m, $\delta = 0.0005$ (i) $\epsilon_r = 2.32$, $t = 0.318, 0.159, 0.0795$ cm; (ii) $\epsilon_r = 9.8$, $t = 0.127, 0.0635, 0.0254$ cm. (From [4], © 1989, IET, reprinted with permission)

and nearly zero in the endfire direction. On the other hand, the crosspolar components are maximum in the endfire direction and nearly zero in the broadside direction.

Varying the feed position alters the relative sizes of the two components. This is illustrated in Fig. 5.14, in which it is observed that, as the feed moved toward the center of the patch, the cross-polarization level increases. Also, as the resonance frequency increases, the quantity $\left| \frac{E_{copol}}{E_{xpol}} \right|$ decreases. The rate of decrease of $\left| \frac{E_{copol}}{E_{xpol}} \right|$ is approximately the same for

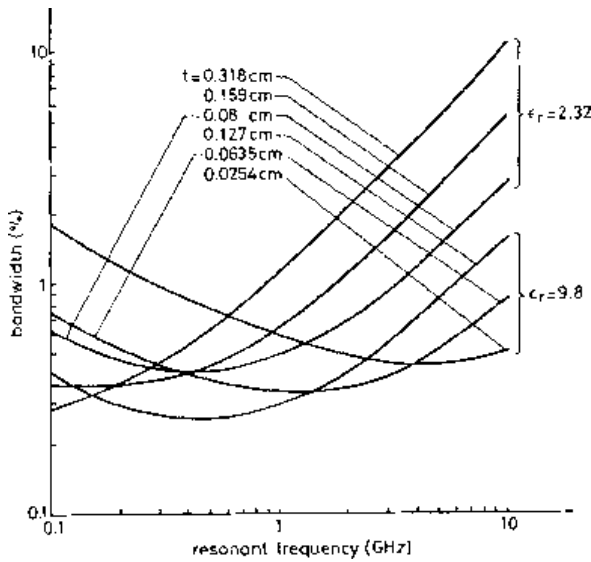


Fig. 5.9 Bandwidth versus resonant frequency for the TM_{11} mode of the circular patch with $\sigma = 5.8 \times 10^7$ S/m, $\delta = 0.0005$ (i) $\epsilon_r = 2.32$, $t = 0.318, 0.159, 0.0795$ cm; (ii) $\epsilon_r = 9.8$, $t = 0.127, 0.0635, 0.0254$ cm. (From [4], © 1989, IET, reprinted with permission)

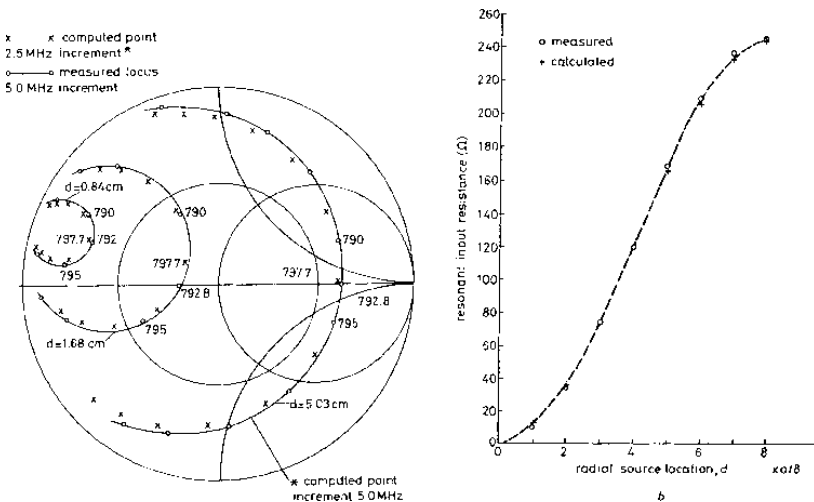


Fig. 5.10 (a) Calculated and measured TM_{11} mode input impedance loci for several radial feed locations. (b) Variation of TM_{11} resonant input resistance with radial feed position for a circular patch with $a = 6.7$ cm on Rexolite 2200 substrate ($\epsilon_r = 2.62$) of thickness 0.159 cm. (From [4]. © 1981 IEEE Reprinted with permission.)

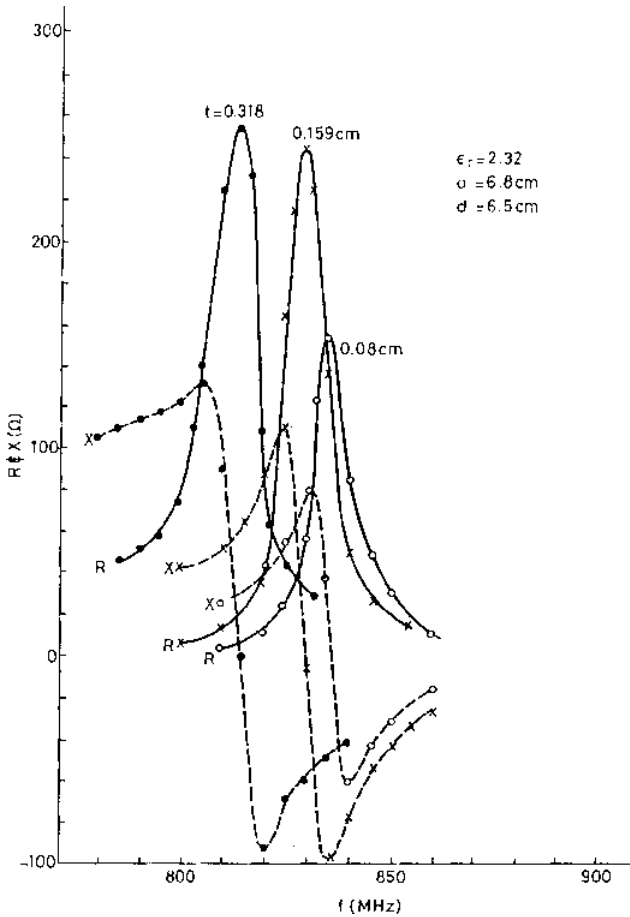


Fig. 5.11 Measured real part (R) and imaginary part (X) of input impedance as function of frequency for the TM_{11} mode of a circular patch with $a = 6.8$ cm, $\epsilon_r = 2.32$ and three dielectric thickness. The feed is at $d = 6.5$ cm. (From [6] © 1983 IEEE Reprinted with permission.)

various feed positions. This feature resembles the results for a rectangular patch [9].

Figure 5.15 shows the results for three different substrate thicknesses. It is noted that $\left| \frac{E_{copol}}{E_{xpol}} \right|$ increases with decreasing substrate thickness. Figure 5.16 is basically the same as Fig. 5.15 except that $\epsilon_r = 9.8$ instead of 2.32. It is observed that a high ϵ_r can improve the ratio $\left| \frac{E_{copol}}{E_{xpol}} \right|$.

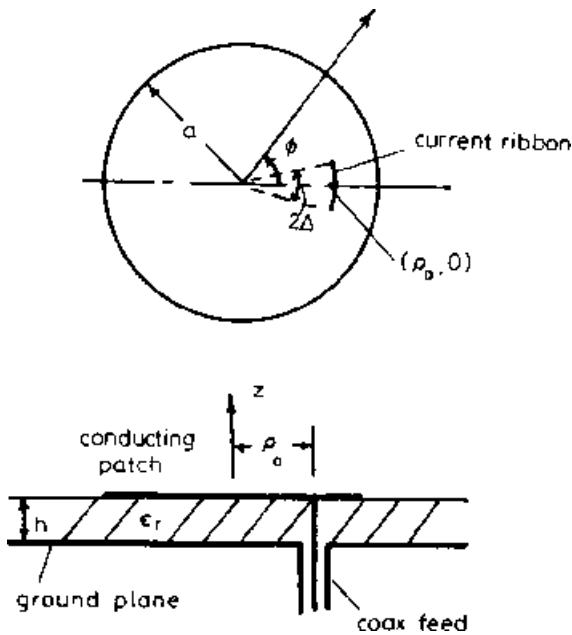


Fig. 5.12 The coordinate system used in the cross polarization study.

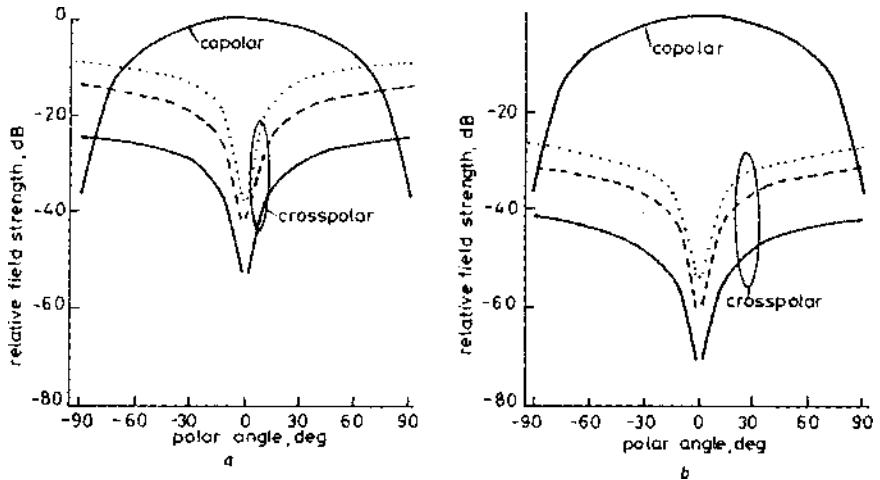


Fig. 5.13 Radiation patterns in $\phi = 90^\circ$ plane. $\epsilon_r = 2.32$, $h = 1.59$ mm. (a) Feed at $\rho_0/a = 0.1$, (b) Feed at $\rho_0/a = 0.9$ (From [7]. © 1992 IET Reprinted with permission.)

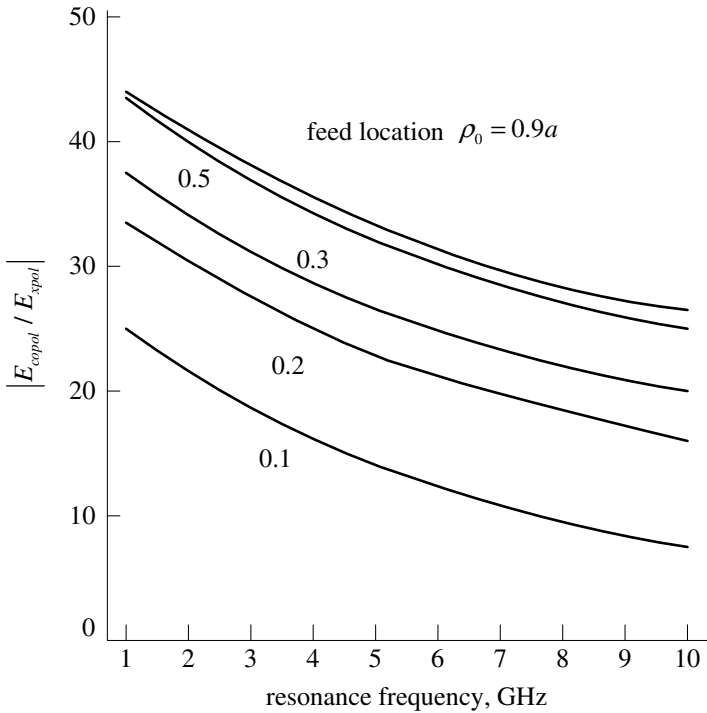


Fig. 5.14 $|E_{copol} / E_{xpol}|$ as function of resonance frequency for different feed positions. $\epsilon_r = 2.32$, $h = 1.9$ mm, $\phi = 90^\circ$ (From [7]. © 1992 IET Reprinted with permission.)

The above results are for the H plane. The ratio $|E_{copol} / E_{xpol}|$ for a number of planes defined by $\phi = 15^\circ$, 30° , 45° , and 75° are indicated by crosses in Fig. 5.17. It is seen that the crosspolarization level is maximum in the plane $\phi = 45^\circ$.

5.6 Problems and Projects

5.6.1 Problems

1. Verify equations (5.22) and (5.23).
2. Verify equations (5.26)–(5.30).
3. Verify equations (5.31) and (5.32).

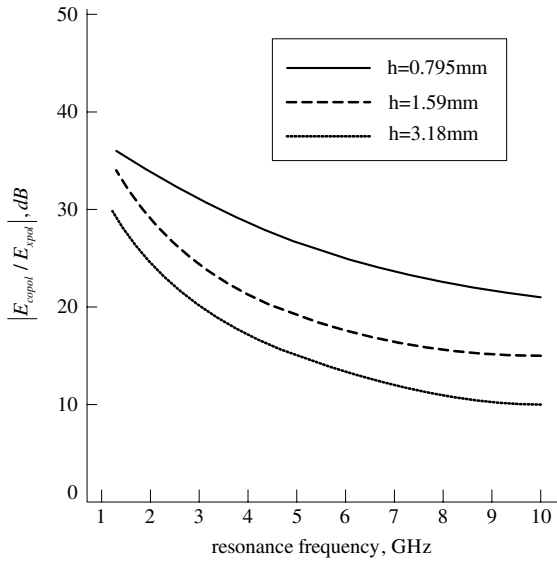


Fig. 5.15 $|E_{copol}/E_{xpol}|$ as function of resonance frequency for different substrate thickness; $\epsilon_r = 2.32$, $\rho_o/a = 0.2$, $\phi = 90^\circ$ (From [7]. © 1992 IET Reprinted with permission.)

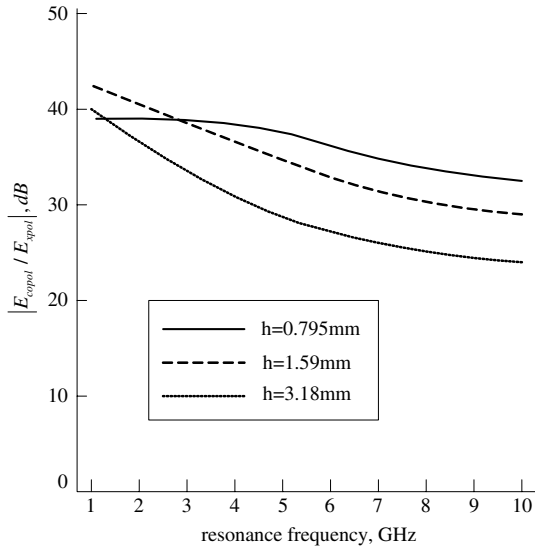


Fig. 5.16 $|E_{copol}/E_{xpol}|$ as function of resonance frequency for different substrate thickness; $\epsilon_r = 9.8$, $\rho_o/a = 0.2$, $\phi = 90^\circ$ (From [7]. © 1992 IET Reprinted with permission.)

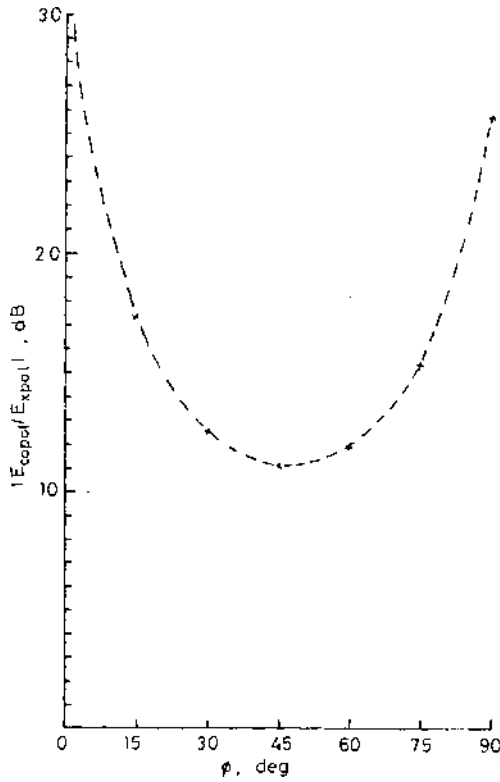


Fig. 5.17 $\left| \frac{E_{copol}}{E_{xpol}} \right|$ in planes defined by various values of ϕ : $\epsilon_r = 2.32$, $h = 1.59$ mm, $f_{11} = 3$ GHz, $\rho_o/a = 0.2$ (From [7]. © 1992 IET Reprinted with permission.)

5.6.2 Projects

(Use the Zeland IE3D or another simulation software)

1. (a) Determine the radius of a circular patch to resonate at the TM_{11} mode at the GPS frequency of 1176 MHz. The substrate permittivity $\epsilon_r = 2.32$. For substrate thickness $t = 1.59$ mm,
 - (i) obtain curves of input resistance R and input reactance X versus frequency for several feed positions.
 - (ii) for the feed position with resonant resistance equal to 50 ohms, obtain the VSWR versus frequency curve and determine the percentage bandwidth, as defined by $VSWR < 2$.

- (b) Repeat (a) for $t = 3.18$ mm.
 - (c) Determine the maximum bandwidth obtainable for the TM_{11} mode by increasing the substrate thickness. You will need to alter the dimensions and the feed position that yields 50 ohms for each thickness.
2. Repeat project 1 for the case of foam substrate with $\varepsilon_r = 1.06$.

References

- [1] A. G. Derneryd, "Analysis of the microstrip disk antenna element," *IEEE Trans. Antennas Propagat.*, Vol. AP-27, pp. 660–664, 1979.
- [2] I. J. Bahl and P. Bhartia, *Microstrip Antennas*, Chapter 3, Artech House, 1980.
- [3] Y. T. Lo, D. Solomon, and W. F. Richards, "Theory and experiment on microstrip antennas," *IEEE Trans. Antennas Propagat.*, Vol. AP-27, pp. 137–145, 1979.
- [4] K. F. Lee and J. S. Dahele, "Characteristics of microstrip patch antennas and some methods of improving frequency agility and bandwidth," In *Handbook of Microstrip Antennas*, J. R. James and P. S. Hall (Editors), Peter Peregrinus, Ltd., London, 1989.
- [5] W. F. Richards, Y. T. Lo and D. D. Harrison, "An improved theory for microstrip antennas and applications," *IEEE Trans. Antennas Propagat.*, Vol. AP-29, pp. 38–46, 1981.
- [6] J. S. Dahele and K. F. Lee, "Effect of substrate thickness on the performance of a circular-disk microstrip antenna," *IEEE Trans. Antennas Propagat.*, Vol. AP-31, pp. 358–360, 1983.
- [7] K. F. Lee, K. M. Luk and P. Y. Tam, "Crosspolarization characteristics of circular patch antenna," *Electron. Lett.*, Vol. 28, pp. 587–589, 1992.
- [8] A. C. Ludwig, "The definition of cross polarization," *IEEE Trans. Antennas Propagat.*, Vol. AP-21, pp. 116–119, 1973.
- [9] T. Huynh, K. F. Lee and R. Q. Lee, "Crosspolarisation characteristics of rectangular patch antennas," *Electron. Lett.*, Vol. 24, pp. 463–464, 1988.